Yin, Y., Sun, Y., Yu, M., Liu, X., Yang, B., Liu, D., Liu, S., Cao, W., & Ashfold, M. N. R. (2014). Arrays of nanorods composed of ZnO nanodots exhibiting enhanced UV emission and stability. *Nanoscale*, *6*(18), 10746-10751. https://doi.org/10.1039/c4nr01558d

Journal Name

RSCPublishing

ARTICLE

# Arrays of Nanorods Composed of ZnO Nanodots Exhibiting Enhanced UV Emission and Stability

Cite this: DOI: 10.1039/xoxxoooooox

Y. Yin,[a] Y. Sun,*[a] M. Yu,*[b] X. Liu,[a] B. Yang,[a] D. Liu,[c] S. Liu,[c] W. Cao[a,d] and Michael N R Ashfold*[e]

Received ooth January 2012,
Accepted ooth January 2012

DOI: 10.1039/xoxxoooooox

www.rsc.org/

A novel one-step coating and assembly approach for fabricating well-defined ZnO nanodot/$SiO_2$ nanorod arrays by hydrolysis-recrystallization growth from 1-D ZnO nanorods is described. The resultant composite nanorod arrays exhibit much enhanced UV emission efficiencies and excellent stability, and thus offer particular promise for application in UV emission devices operating in harsh environments.

## Introduction

Nanorod (NR) arrays of many different nanomaterials have been shown to have significant applications in light emission devices,[1] biosensors,[2] solar cells,[3,4] piezoelectric generators,[5,6] photocatalysis,[7,8] field emission devices,[9] etc. – reflecting their advanced functional properties and the feasibility of their incorporation within nanodevices. Compared to NRs, nanodots (NDs) typically possess yet higher surface area to volume ratios, and superior size-control – thereby enabling improved performance in a range of different applications.[10-14] However, the instability and deterioration of NDs induced by aggregation and loss, as well as the difficulties associated with aligning and packing NDs, imposes some constraints on their practical utility. To this end, it could clearly be advantageous to combine NRs with NDs and thereby integrate the advantages of both types of nanostructure in a single entity. The very recent literature contains several reports of NRs (and nanotubes) decorated by NDs and their possible application in quantum dot-sensitized solar cells,[15] in photocatalysts,[16] in bio-sensing [17] and in single-photon sources.[18]

The family of nanoscale zinc oxide (ZnO) structures, including ZnO nanorods/nanowires,[19-22] nanotubes,[23] nanobelts [24] and nanodots,[25] has stimulated huge interest over the last decade.[26-28] ZnO NDs have attracted particular attention, given their size and possible quantum confinement effects, and have shown performance in light emission devices [29,30] and in cell labeling.[31] Silicon oxide ($SiO_2$) has been employed as a shield, with the aim of improving the optical properties and stability of ZnO nanomaterials.[32-35] Previous studies have reported that $SiO_2$-coated ZnO NRs display high sensitivity towards detecting ultraviolet (UV) photons [36] and biomolecules,[37] good UV-durable superhydrophobicity,[38] and enhanced UV emission.[39,40] Conversely, heterogeneous ZnO ND/$SiO_2$ structures reportedly show enhanced visible emission [41] but negative photoconductivity.[42] It may be relevant to note that in most such studies reported to date, the ZnO NDs were either embedded in bulk $SiO_2$ or individual silica-coated ZnO NDs were randomly distributed in solution.

Here we describe a new, easy-to-implement, high-yield route to forming well-defined ZnO/$SiO_2$ NR arrays, wherein the ZnO NDs are neatly packaged inside a $SiO_2$ NR matrix, using a direct one-step treatment of bare, ultra-thin ZnO NRs. The resulting heterogeneous nanostructure, which combines the merits of zero-dimensional (0-D) NDs and 1-D NRs of ZnO, exhibit much enhanced UV photoluminescence (PL) emission efficiency and greatly improved stability in solution (*cf*. the pre-treated NRs). This synthetic strategy constitutes a new 'top-down' route to achieving 1-D assemblies of 0-D nanomaterials with improved properties for practical applications.

## Experimental

<002>-aligned ZnO seed layers were deposited on Si(100) substrates by sputtering from a ZnO target (99.99%). High purity argon (at a flow rate, $F$ = 80 sccm) and oxygen ($F$ = 20 sccm) were used as the sputter gas at a fixed pressure of 1 Pa. The sputter deposition was carried out with a target-substrate distance of 50 mm, a radio frequency power of 160 W and a substrate temperature of 400°C, for a duration of 5 min.

Ultra-thin ZnO NR arrays were synthesized on the ZnO seed layers by hydrothermal growth. 0.002 M aqueous solutions of zinc nitrate and hexamethylenetetramine were separately heated at 90°C in a thermostatically controlled oil bath for 30 min. 50 ml of each solution was then mixed in a glass bottle, into which the substrate was then immediately immersed, and the bottle sealed. The sample was then maintained at 90°C for 3 hrs, then removed, rinsed with deionized water and then dried using a freeze dryer (TFD550J, I1shin Lab, Korea).

60 mL of dehydrated ethanol and 50-500 μL of tetraethylorthosilicate (TEOS) were first mixed and stirred at room temperature for 30 min, at which point the ZnO NR array covered substrates were immersed in the solution. 3 mL of ammonia solution (25-28%) was added and the solution sealed and stirred for 3 hrs. The resulting samples were cleaned with ethanol and water, and then dried in the freeze dryer.

The as-grown products were characterized and analyzed by scanning electron microscopy (SEM: FEI, Quanta 200F),

transmission electron microscopy (TEM: FEI, Tecnai-G2-F30) and by X-ray diffraction (XRD: Bruker, D8 Advance, with Cu Kα radiation). PL spectra were measured using a spectrofluorometer (HORIBA, Fluoromax-4, at an excitation wavelength of 325 nm).

## Results and discussion

The fabrication strategy for the ZnO ND/$SiO_2$ NR arrays relies on the corrosive effect of ammonia on ultra-thin ZnO NRs grown by hydrothermal methods. Figure 1a shows top (main figure) and cross-sectional (inset) SEM images of the initial ZnO NR sample, revealing an extended array of well-aligned, evenly distributed NRs with diameters in the range 20-25 nm and average lengths ~1.5 μm. These ultra-thin NRs are very reactive in an ethanol / ammonia mixture and disappear from the substrate within 3 hrs if left in such a solution – consistent with previous studies showing the decomposition of thin ZnO NRs into tubular structures in an ammonia solution.[43,44] We therefore sought to design a one-step method based on hydrolysis in TEOS / ammonia mixtures, whereby the ultra-thin NRs would be both etched and silica-coated with the ammonia playing a dual role by supplying $OH^-$ species that both catalyze the hydrolysis of TEOS and, at the same time, encourage decomposition of the NRs. Tuning the TEOS concentration would then offer some control of the silica formation process and the extent and speed of the etching reaction.

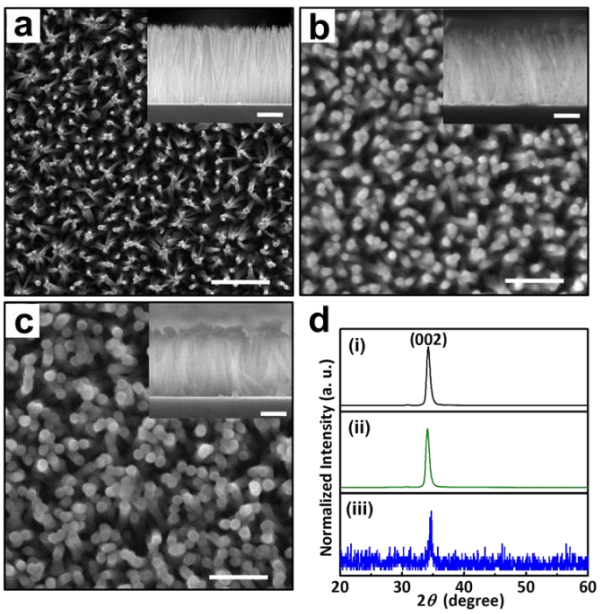


**Fig. 1** SEM images of (a) the bare NR array and of the NR arrays treated with, respectively, (b) 100 μL and (c) 500 μL of TEOS. Each panel displays a plan view image, with a cross-sectional view as an inset. The scale bar in each image is 500 nm. XRD spectra of these three samples are shown, in order, as traces (i) – (iii) in panel (d).

To test this ambition, bare NR arrays were immersed in premixed solutions comprising 60 mL of dehydrated ethanol containing between 50 and 500 μL of TEOS. 3 mL of aqueous ammonia solution (25-28%) was then added, and stirring continued for 3 hrs as described above. SEM images of the NR samples treated with solutions containing 100 μL and 500 μL of TEOS are presented in Figures 1b and 1c. These images show that the individual NRs and the ordered array structure survive this processing, though the NR diameters increase, to an extent that scales with the amount of TEOS used. XRD patterns of the bare NR sample and of samples treated with, respectively, 100 μL and 500 μL of TEOS are shown in Figure 1d. Consistent with the SEM results, the dominance of the ZnO (002) reflection confirms the ordered alignment of the bare NRs. Given (i), the SEM images, which show that TEOS treatment does not degrade the overall NR alignment, and (ii) the realisation that the underlying <002>-aligned seed layer must make some contribution to all of the measured XRD spectra, the reduced (002) peak intensities from the TEOS-treated samples suggests that such processing affects the encapsulated ZnO material.

TEM was employed to reveal further details. The diameter of a single bare NR (Figure 2a) is measured as ~25 nm. The high-resolution (HR) TEM image (Figure 2b) of a bare NR presents a smooth and continuous surface, and parallel crystal planes spaced by 0.26 nm – characteristic of ZnO (002) planes – oriented normal to the NR growth direction. TEM images of NRs treated with 100 μL of TEOS (Figure 2c) exhibit a core-shell structure, with an overall diameter of ~50 nm that includes a ~15 nm thick annular silica shell. Similar data was obtained for NRs treated with 50 μL of TEOS (see Figure S1 in the electronic supplementary information (ESI)). Interestingly, and in contrast to the relatively straight edge profiles of the bare NRs, the interface between the core ZnO NR and the silica shell appears 'lumpy'. Some dark nanoparticles are evident in the silica shell and aligned around the NR core. The HRTEM image shown in Figure 2d confirms that the core NR and the adjacent nanoparticles are ZnO, but with different crystal orientations – validating the initial premise that TEOS treatment could offer an effective route to modifying the morphology of the ultra-thin ZnO NRs whilst, at the same time, shielding them from complete dissolution. Yet more strikingly, as Figure 2e shows, samples treated with 500 μL of TEOS still retain their NR morphology, though the total diameter is further enlarged, to ~100 nm. Under these conditions, HRTEM analysis suggests that the ZnO core within each $SiO_2$ shell has decomposed, yielding a densely-packed set of NDs with diameters in the range of 3-8 nm (see Figure S2). Figure 2f shows two such embedded nanoparticles, that exhibit different lattice spacings (0.28 nm and 0.26 nm, matching the (100) and (002) plane spacings in ZnO, respectively), consistent with formation of ZnO ND-containing $SiO_2$ NRs.

Most ZnO NDs reported previously were produced by wet chemical methods [25,31] or by pulsed laser deposition.[30] The present ZnO NDs, in contrast, have evolved from ultra-thin NRs as a result of the etching effect of ammonia in combination with the influence of TEOS during silica coating. Evidently, the silica shell protects the ZnO NR from rapid decomposition, enabling retention of the global NR morphology. Previous studies of silica shells formed by hydrolysing TEOS have revealed a mesoporous structure, containing many nanosized pores.[45] We can envisage two limiting routes to forming the observed ND-containing $SiO_2$ NRs. Both assume that, during TEOS treatment, the pre-formed NRs are etched by the alkaline solution and that the decomposition products diffuse into the nanosized pores within the growing silica layer. In model (1), the observed NDs are pictured as surviving nanosized debris from localised dissolution of the pre-formed NRs. Model (2), in contrast, assumes essentially complete dissolution of material removed from the NR, and that the observed NDs arise as a

 

result of subsequent condensation and recrystallization within the pores. We favour growth model (2) for several reasons: Given that ND diffusion within the silica shell is likely to be limited, the uniformity of the ND size distribution within the $SiO_2$ NRs (Figure 2e) would be rather surprising if the NDs were simply debris from disintegration of a NR. The range of orientations presented (*e.g.* Figures 2d and 2f) also mitigates against model (1). Had the observed NDs simply broken away from the pre-existing NR, we might expect them to present similar orientations to the original ZnO NR (or to other nearby NDs in the case that the imaged NDs are secondary NDs arising from the disintegration of a larger primary particle). On balance, therefore, we favor a ND formation mechanism (model (2)) wherein water soluble decomposition species (*e.g.* $[Zn(OH)_3]^-$, $[Zn(OH)_4]^{2-}$, *etc*) diffuse into the growing silica layer through the nanosized pores, which guide the subsequent condensation and recrystallization, and eventual formation of the ZnO ND/$SiO_2$ NR arrays. Recrystallization is confined to the pores (not the bulk solution) on concentration grounds, and may well be encouraged by nucleation on larger clusters arising in the NR dissolution (*i.e.* a hybrid mechanism involving recrystallization (model (2)) based on embryonic seeds formed as in model (1)). Diffusive loss from the ZnO NR core ceases once the available vacancies in the adjacent $SiO_2$ matrix are fully occupied; the outermost pure silica shell should then prevent further loss of ZnO species and also help protect the ZnO/$SiO_2$ NRs from harsh external environments.

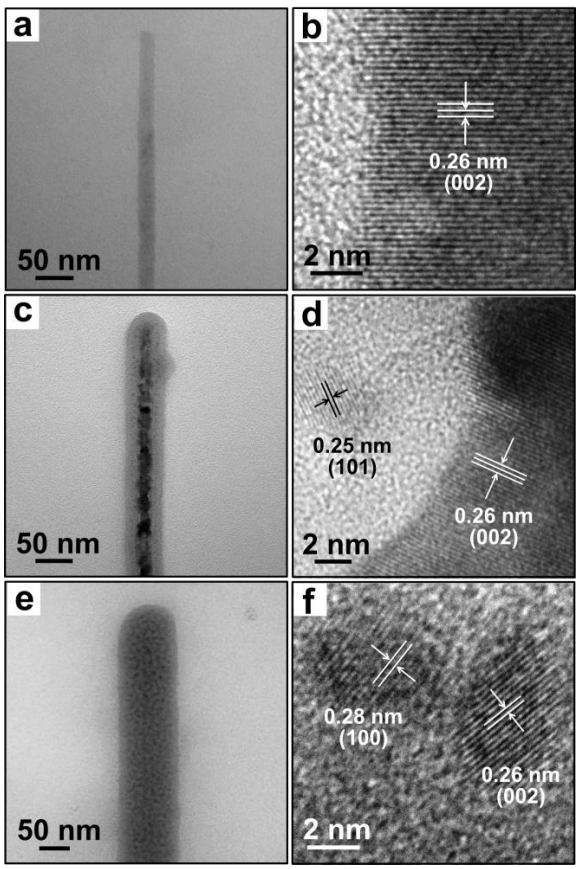


**Fig. 2** Normal and high-resolution TEM images of a bare NR ((a) and (b)) and of NRs treated with 100 μL ((c) and (d)) and 500 μL TEOS ((e) and (f)), respectively.

PL spectra of the bare ZnO NR array and from TEOS treated NR samples following 325 nm excitation (3 × 8 $mm^2$ area in each case) are shown in Figure 3. All show an intense, sharp near-band-edge UV emission feature centred at 382 nm together with a weak, broad visible emission band (to which we return later) that is traditionally ascribed to various defects and impurities.[46] The very high UV to visible intensity ratio ($I_{UV}/I_{visible}$) exhibited by all of these samples indicates the high crystal quality of the ZnO samples. Analysis of dozens of groups of both bare and TEOS treated NR samples confirms that TEOS treatment leads to an increase in $I_{UV}$ and that the degree of enhancement scales with the TEOS concentration. NR samples treated with 500 μL of TEOS displayed UV emission intensities that ranged from 70-200% larger than that from the untreated NR samples (see Figure 4).

The literature contains many reports of PL from ZnO NDs (and nanoparticles) produced by wet chemical methods, almost all of which show strong visible emission but very weak (or even a complete lack of) UV emission [31,35,47] as a result of defects and/or of adsorbed impurities. The ZnO ND/$SiO_2$ NR arrays prepared in the present work, in contrast, show strong UV emission features and large $I_{UV}/I_{visible}$ ratios.

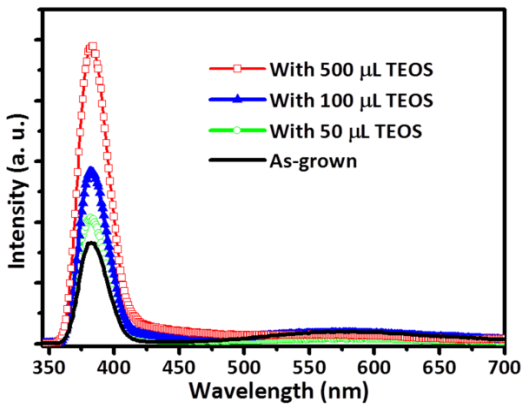


**Fig. 3** Photoluminescence spectra of the bare and TEOS treated ZnO NR arrays.

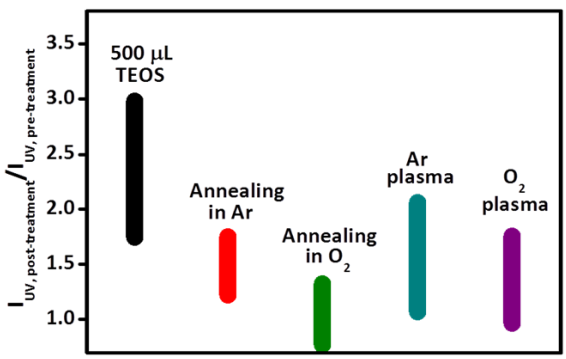


**Fig. 4** Effect of a range of post-processing treatments on the UV emission intensity from ZnO NR samples, expressed in terms of the intensity ratio, $I_{UV,\ post\text{-}treatment}/I_{UV,\ pre\text{-}treatment}$.

Plasma processing and annealing can be effective post-treatment strategies for enhancing the intensity of UV emission from ZnO NRs.[48,49] The UV emission from the bare ZnO NRs grown in the present work is already rather strong, and the maximum UV emission enhancement achieved using either of

these 'traditional' post-processing treatments was only ~80%, as shown in Figure 4. Hydrolysis with 500 μL of TEOS, in contrast, results in UV emission intensity increases as large as ~200%. Previous studies have shown high UV PL efficiencies from ZnO samples with high surface to volume ratio when the surface defects are passivated.[50] $SiO_2$ coating has also been suggested not just to boost the probability of UV emission but also to reduce the surface-trap-related visible emission through formation of Zn–O–Si bonds on the surface of ZnO samples.[40] Further, given the small diameters of the ZnO nanodots, it is quite likely that the exciton emission is being enhanced by quantum confinement effects (QCEs). Based on these results, we suggest that the substantial increase in UV emission intensity as the ZnO NRs evolve to ZnO NDs embedded in a $SiO_2$ shell can be traced to a combination of QCEs, the large increase in surface to volume ratio, and passivation of the ZnO-silica interface by formation of stabilizing ≡Zn−O−Si≡ bonds in the condensation process. Concurrently, the crystallinity of the ZnO NDs and the passivation of their surfaces are sufficient to minimise the intensity of the defect-related green-red emission.

To examine the stability of the ZnO/$SiO_2$ NRs in solution, we investigated the 325 nm laser induced PL spectra of both the bare and the TEOS treated NR samples before and after immersion in various pH buffer solutions for various times, *t*. The bare NRs were found to lose ~97% of the original UV emission intensity after immersion in an aqueous buffer solution of pH = 4.00 for just *t* = 15 min, while the NR samples treated with 50 μL and 100 μL of TEOS maintained ~30% of their original emission intensity even after immersion for *t* = 3 hrs. The sample treated with 500 μL of TEOS showed the best performance, with almost no loss of emission intensity over a 3 hr time period (see Figure 5). Similar immersion experiments with an aqueous buffer solution of pH = 9.18 again demonstrated that the stability of the TEOS treated NRs is far superior to that of the bare NRs (see Figure S5).

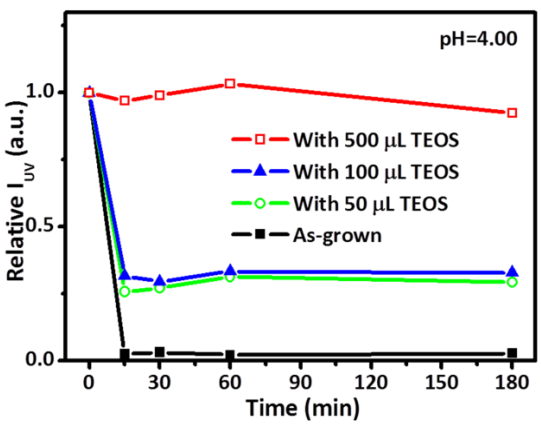


**Fig. 5** Time dependence of the relative UV emission intensity of the bare and TEOS treated ZnO NRs after immersion in an aqueous buffer solution with pH = 4.00.

As Figure 3 showed, the ZnO ND/$SiO_2$ NR samples exhibit weak blue emission (in the 400-500 nm region) in addition to a broader visible emission (spanning the green to red spectral region). Emission centred at ~520 nm within the latter is usually assigned to defects of oxygen vacancies, while the longer wavelength emission (maximising in the 570-610 nm range) is traditionally associated with defects based on oxygen interstitials.[48] The intensity of the former (blue) emission, in contrast, is seen to increase with the amount of TEOS used in the silica-coating process (Figure 3), and is thus attributed to the amorphous silica shells (see Figure S6).

Figure 6 shows how the PL emission from ZnO ND/$SiO_2$ NR samples is affected by annealing in an $O_2$ atmosphere. Annealing ZnO ND/$SiO_2$ NR samples treated with 500 μL of TEOS in an $O_2$ atmosphere at 300°C leads to enhanced emission centred at ~475 nm, which gains in intensity and blue-shifts (to a centre wavelength ~450 nm) in samples annealed at 600°C, but this emission is completely eliminated by annealing in $O_2$ at 900°C. Blue emission has been reported from ZnO/$SiO_2$ composite samples formed by a range of growth methods, and various origins proposed for the emission (*e.g.* zinc vacancies in the depletion layer near the ZnO/$SiO_2$ interface, recombination between donor (zinc interstitial) – acceptor (zinc vacancy) pairs, and bound excitons).[40,51] The apparent blue shift with increasing annealing temperature hints at the present emission having multiple origins. It is also worth noting that any emission from amorphous silica decreases with increasing annealing temperature (see Figure S7), implying that emission from the silica coating makes little contribution to the blue emission from the ZnO ND/$SiO_2$ NR samples annealed at 300 and 600°C. Most importantly, we re-emphasise that annealing the ZnO ND/$SiO_2$ NR samples in oxygen at 900°C greatly reduces all of the visible emission and leads to some improvement in the UV emission intensity (*cf*. the unannealed sample) – as shown in Figure 6.

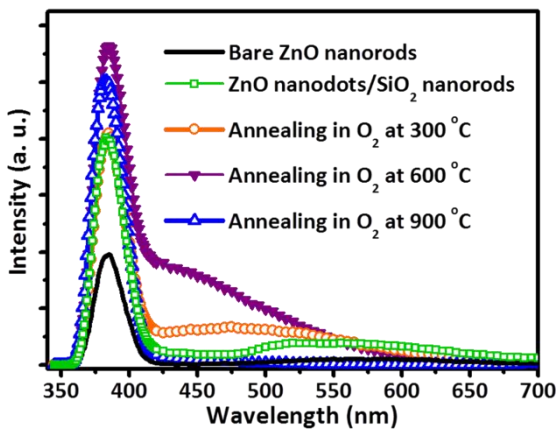


**Fig. 6** PL spectra of the bare ZnO NRs, and of the as-grown and annealed ZnO ND/$SiO_2$ NR samples.

## Conclusions

Arrays of ZnO ND seeded $SiO_2$ NRs have been fabricated from 1-D ZnO NRs by a one-step hydrolysis-recrystallization growth process. Despite the inevitable reduction in overall ZnO content, the resulting composite NR arrays display much enhanced UV emission intensities (up to 3-times that of the bare NRs). The protection and surface passivation benefits afforded by encapsulation in $SiO_2$ have been demonstrated by investigating the UV emission characteristics of these ZnO ND/$SiO_2$ NRs after immersion in aqueous solutions of various pH. Compared with the as-grown ZnO NRs, the ZnO ND/$SiO_2$ NRs also display much improved stability in aqueous solutions, thereby demonstrating their potential for UV emission devices operating in harsh environments. We anticipate that the new 'top-down' growth strategy demonstrated here for the specific case of ZnO ND/$SiO_2$ NRs could likely be applied to the design of other novel-structured nanomaterials in an easy and direct way.

## Acknowledgements

This work was financially supported by the National Natural Science Foundation of China (Grant No.11104046), National Basic Research Program of China (973 Program) (Grant No.2013CB632900), the Fundamental Research Funds for the Central University (Grant Nos. HIT.BRETIII.201216, HIT.BRETIII.201225, and HIT.BRETIV.201313). M.Y. thanks financial support by the Young Thousand Plan, and the authors appreciate the constructive criticisms offered by one reviewer of the original manuscript.

## Notes and references

[a] Condensed Matter Science and Technology Institute, School of Science, Harbin Institute of Technology, Harbin 150080, China
E-mail: sunye@hit.edu.cn
[b] State Key Laboratory of Urban Water Resource and Environment, School of Chemical Engineering and Technology, Harbin Institute of Technology, Harbin 150001, China
E-mail: miaoyu_che@hit.edu.cn
[c] Key Laboratory of Microsystems and Microstructures Manufacturing, Harbin Institute of Technology, Harbin 150080, China
[d] Materials Research Institute, The Pennsylvania State University, University Park, Pennsylvania16802, USA
[e] School of Chemistry, University of Bristol, Bristol BS8 1TS, UK
E-mail: mike.ashfold@bristol.ac.uk

Electronic Supplementary Information (ESI) available: Suggested reaction scheme for the chemical processes occurring in this work; TEM images of ZnO NRs treated with 50 μL of TEOS; the diameter distribution of the ZnO NDs inside the ZnO/$SiO_2$ NRs; PL spectra of as-grown ZnO NRs and of NRs after $O_2$ and Ar plasma treatment; PL spectra of as-grown ZnO NRs and of NRs after annealing in $O_2$ and in Ar; plot showing the time dependence of the relative UV emission intensity of the as-grown ZnO NRs and the TEOS-treated ZnO NRs immersed in an aqueous buffer solution at pH = 9.18; PL spectra of as-grown ZnO NRs and of the silica powders formed by hydrolysis and condensation reactions of TEOS; PL spectra of $SiO_2$ powder after annealing in $O_2$ at 300, 600 and 900°C. See DOI: 10.1039/b000000x/

1 C. Hahn, Z. Zhang, A. Fu, C. H. Wu, Y. J. Hwang, D. J. Gargas, P. Yang, *ACS Nano*, 2011, **5**, 3970.
2 A. Gitsas, B. Yameen, T. D. Lazzara, M. Steinhart, H. Duran, W. Knoll, *Nano Lett.*, 2010, **10**, 2173.
3 J. Jean, S. Chang, P. R. Brown, J. J. Cheng, P. H. Rekemeyer, M. G. Bawendi, S. Gradecak, V. Bulovic, *Adv. Mater.*, 2013, **25**, 2790.
4 C. W. Kung, H. W. Chen, C. Y. Lin, K. C. Huang, R. Vittal, K. C. Ho, *ACS Nano*, 2012, **6**, 7016.
5 M.-Y. Lu, J. Song, M.-P. Lu, C.-Y. Lee, L.-J. Chen, Z. L. Wang, *ACS Nano*, 2009, **3**, 357.
6 Y. Qiu, H. Zhang, L. Hu, D. Yang, L. Wang, B. Wang, J. Ji, G. Liu, X. Liu, J. Lin, F. Li, S. Han, *Nanoscale*, 2012, **4**, 6568.
7 Y. B. Li, T. Takata, D. Cha, K. Takanabe, T. Minegishi, J. Kubota, K. Domen, *Adv. Mater.*, 2013, **25**, 125.
8 F.-H. Chu, C.-W. Huang, C.-L. Hsin, C.-W. Wang, S.-Y. Yu, P.-H. Yeh, W.-W. Wu, *Nanoscale*, 2012, **4**, 1471.
9 H. B. Zeng, X. J. Xu, Y. Bando, U. K. Gautam, T. Y. Zhai, X. S. Fang, B. D. Liu, D. Golberg, *Adv. Funct. Mater.*, 2009, **19**, 3165.
10 S. J. Zhu, Q, N. Meng, L. Wang, J. H. Zhang, Y. B. Song, H. Jin, K. Zhang, H. C. Sun, H. Y. Wang, B. Yang, *Angew. Chem. Int. Ed.*, 2013, **52,** 3953.
11 S. Qu, H. Chen, X. Zheng, J. Cao, X. Liu, *Nanoscale*, 2013, **5**, 5514.
12 Y. Hu, Z. M. Jiang, C. D. Xu, T. Mei, J. Guo, T. White, *J. Phys. Chem. C*, 2007, **27**, 9757.
13 J. Zheng,; J. T. Petty,; R. M. Dickson, *J. Am. Chem. Soc.*, 2003, **125**, 7780.
14 C.-H. Liu, S.-Y. Chen, C.-Y. Chen, J.-H. He, L.-J. Chen, J. C. Ho, Y.-L. Chueh, *ACS Nano*, 2011, **5**, 6637.
15 R. S. Selinsky, Q. Ding, M. S. Faber, J. C. Wright, S. Jin, *Chem. Soc. Rev.*, 2013, **42**, 2963.
16 X. Zhang, C. Shao, Z. Zhang, J. Li, P. Zhang, M. Zhang, J. Mu, Z. Guo, P. Liang, Y. Liu, *ACS Appl. Mater. Interfaces*, 2012, **4**, 785.
17 H. B. Tang, G. W. Meng, Q. Huang, Z. Zhang, Z. L. Huang, C. H. Zhu, *Adv. Funct. Mater.*, 2012, **22**, 218.
18 E. Uccelli, J. Arbiol, J. R. Morante, A. F. Morral, *ACS Nano*, 2010, **4**, 5985.
19 L. Vayssieres, *Adv. Mater.*, 2003, **15**, 464.
20 Y. Sun, N. A. Fox, D. J. Riley, M. N. R. Ashfold, *J. Phys. Chem. C*, 2008, **112**, 9234.
21 D. Tsivion, M. Schvartzman, R. Popovitz-Biro, E. Joselevich, *ACS Nano*, 2012, **6**, 6433.
22 L. S. Wang, D. Tsan, B. Stoeber, K. Walus, *Adv. Mater.*, 2012, **24**, 3999.
23 Y. Sun, G. M. Fuge, N. A. Fox, D. J. Riley, M. N. R. Ashfold, *Adv. Mater.*, 2005, **17**, 2477.
24 M. Lucas, W. J. Mai, R. S. Yang, Z. L. Wang, E. Riedo, *Nano Lett.*, 2007, **7**, 1314.
25 C. Pacholski, A. Kornowski, H. Weller, *Angew. Chem., Int. Ed.*, 2002, **41**, 1188.
26 L. Schmidt-Mende, J. L. MacManus-Driscoll, *Mater. Today*, 2007, **10**, 40.
27 Xu, S. Wang, Z. L. *Nano Res.*, 2011, **4**, 1013-1098.
28 J. L. Gomez, O. Tigli, *J. Mater. Sci.*, 2013, **48**, 612.
29 C. H. Bae, S. M. Park, S. C. Park, J. S. Ha, *Nanotechnology*, 2006, **17**, 381.
30 S. K. Lee, J. Y. Son, *Appl. Phys. Lett.*, 2012, **100**, 132109.
31 X. S. Tang, E. S. G. Choo, L. Li, J. Ding, J. M. Xue, *Chem. Mater.*, 2010, **22**, 3383.
32 M. S. Sadjadi, N. Farhadyar, K. Zare, *J. Nanosci. Nanotech.*, 2011, **11**, 9034.
33 Y. Q. Li, Y. Yang, S. Y. Fu, X. Y. Yi, L. C. Wang, H. D. Chen, *J. Phys. Chem. C*, 2008, **112**, 18616.
34 S. Panigrahi, A. Bera, D. Basak, *J. Colloid Interface Sci*., 2011, **353**, 30.
35 H. M. Yang, Y. Xiao, K. Liu, Q. M. Feng, *J. Am. Ceram. Soc.*, 2008, **91**, 1591.
36 M. Afsal, C. Y. Wang, L. W. Chu, O. Y. Hao, L. J. Chen, *J. Mater. Chem.*, 2012, **22**, 8420.
37 J. W. Zhao, L. Z. Wu, J. F. Zhi, *J. Mater. Chem.*, 2008, **18**, 2459.
38 L. L. Wang, X. T. Zhang, Y. Fu, B. Li, Y. C. Liu, *Langmuir*, 2009, **25**, 13619.
39 B. H. Chu, L. C. Leu, C. Y. Chang, F. Lugo, D. Norton, T. Lele, B. Keselowsky, S. J. Pearton, F. Ren, *Appl. Phys. Lett.*, 2008, **93**, 233111.
40 S. Panigrahi, D. Basak, *Chem. Phys. Lett.*, 2011, **511**, 91.
41 N. Hagura, T. Takeuchi, S. Takayama, F. Iskandar, K. Okuyama, *J. Lumin*., 2011, **131**, 138.
42 S. Panigrahi, A. Bera, D. Basak, *ACS Appl. Mater. & Interfaces*, 2009, **1**, 2408.
43 Y. S. Han, L. W. Lin, M. Fuji, M. Takahashi, *Chem. Lett.*, 2007, **36**, 1002.
44 X. F. Ma, M. J. Gao, J. B. Zheng, H. Z. Xu, G. Li, *Phys. E*, 2010, **42**, 2237.
45 H. J. Zhang, J. Wu, L. P. Zhou, D. Y. Zhang, L. M. Qi, *Langmuir*, 2007, **23**, 1107.
46 C. Klingshirn, J. Fallert, H. Zhou, J. Sartor, C. Thiele, F. Maier-Flaig, D. Schneider, H. Kalt, *Phys. Status Solidi B*, 2010, **247**, 1424.
47 A. Asok, A. R. Kulkarni, M. N. Gandhia, *J. Mater. Chem. C*, 2014, **2**, 1691.
48 Y. Sun, N. G. Ndifor-Angwafor, D. J. Riley, M. N. R. Ashfold, *Chem. Phys. Lett.*, 2006, **431**, 352.
49 C. Baratto, E. Comini, M. Ferroni, G. Faglia, G. Sberveglieri, *CrystEngComm*, 2013, **15**, 7981.
50 Y. Sun, M. N. R. Ashfold, *Nanotechnology*, 2007, **18**, 245701.
51 Y.-Y. Peng, T.-E. Hsieh, C.-H. Hsu, *Nanotechnology*, 2006, **17**, 174.